*magnetochemistry*

MDPI

*Article*

# Exploring the Potential of Oxalyldihydrazide-Derived Schiff Bases as Versatile Ligands: Synthesis, Structural Characterization, and Magnetic Properties

**Ernesto Costa-Villén [1], Marina Ortiz [1], Pedro Sitjar [1], Cristina Puigjaner [2] and Mohamed Salah El Fallah [1,3,*]**

[1] Departament de Química Inorgànica i Organica, Secció Inorgànica, Universitat de Barcelona, Barcelona Marti i Franquès, 1-11, 08028 Barcelona, Spain; ecostavillen@ub.edu (E.C.-V.); mortizme8@alumnes.ub.edu (M.O.); psitjabo7@alumnes.ub.edu (P.S.)
[2] Departament de Mineralogia, Cristal·lografia i Dipòsits Minerals and Unitat de Difracció de R-X, Centre Científic i Tecnològic de la Universitat de Barcelona (CCiT-UB), Universitat de Barcelona, 08028 Barcelona, Spain; cris@ccit.ub.edu
[3] Institut de Nanociència i Nanotecnologia (IN2UB), Universitat de Barcelona, 08028 Barcelona, Spain
* Correspondence: salah.elfallah@qi.ub.es

**Abstract:** Schiff bases constitute a broad and well-established class of ligands widely utilized in coordination chemistry. To further enrich this family and assess the potential impact of oxalyldihydrazide-derived Schiff bases in the realms of coordination chemistry and molecular magnetism, three novel ligands have been synthesized and investigated. i.e., N′1,N′2-bis((*E*)-pyridin-2-ylmethylene)oxalohydrazide (**$H_2$L1**), N′1-((*E*)-(3-methylpyridin-2-yl)methylene)-N′2-((*E*)-(6-methylpyridin-2-yl)methylene)oxalohydrazide (**$H_2$L2**) and N′1,N′2-bis((E)-phenyl(pyridin-2-yl)methylene)oxalohydrazide (**$H_2$L3**) were synthesized and then combined with various 3*d* metals, resulting in the formation of five new complexes with formula $[Cu_5(L1)_2(H_2O)_8(MeOH)_2(NO_3)_2](NO_3)_4$ (**1**), $[Mn_2(HL2)_2(BzO)_2(MeOH)_2]\cdot 2MeOH$ (**2**), $[Ni(HL2)_2]\cdot 2MeOH$ (**3**), $[Ni_4(L2)_4]\cdot 4MeOH$ (**4**), $[Ni_8(L3)_4(AcO)_4(H_2O)_{12}](OAc)_4$ (**5**). These compounds were structurally and magnetically characterized, revealing the various coordination modes exhibited by the ligands and a distinct antiferromagnetic behavior. Alternating current (AC) susceptibility measurements were conducted on complex **1**, showing no evidence of Single Molecule Magnet (SMM) behavior.

**Keywords:** oxalyldihydrazide; Schiff bases; synthesis; coordination chemistry; magnetism



Academic Editor: Marius Andruh

Received: 24 October 2024
Revised: 4 January 2025
Accepted: 6 January 2025
Published: 13 January 2025

**Citation:** Costa-Villén, E.; Ortiz, M.; Sitjar, P.; Puigjaner, C.; El Fallah, M.S. Exploring the Potential of Oxalyldihydrazide-Derived Schiff Bases as Versatile Ligands: Synthesis, Structural Characterization, and Magnetic Properties. *Magnetochemistry* **2025**, *11*, 4. https://doi.org/10.3390/magnetochemistry11010004



## 1. Introduction

Molecular magnetism is a well-established research field that has been ongoing for a long time. It was in 1993 when Sessoli et al. [1] discovered the ability of the $Mn_{12}$-acetate molecule to retain its magnetization once the magnetic field is removed and behaves as a Single Molecule Magnet (SMM). Since then, many researchers have focused their efforts on synthesizing new molecules that exhibit slow relaxation of magnetization (SRM) containing transition metals, such as $[V(IV)O]^{2+}$ [2], Mn(II) [3,4], Fe(II/III) [5,6], Co(II) [7,8], Cu(II) [9], or Ag(II) [10], rare-earth metals, especially $Tb(III)^{+}$ [11–13] and Dy(III) [12–14], who possess strong magnetic anisotropy, the combination of 3*d*/4*f* metals [15–20], and even a few cases of actinide-derived compounds containing Th(III) [20] and $[U(V)O]^{2+}$ [21,22]. The purpose of synthesizing these compounds is to leverage their quantum properties for applications in Quantum Information Processing (QIP) technologies such as quantum storage devices [23], qubits [24,25], or spintronics [26,27].

To achieve this ambitious goal, Schiff bases, formed through the condensation of a primary amine group (R–$NH_2$) and a carbonyl group, i.e., a ketone (RR′–C=O) or an aldehyde (RH–C=O), are attractive candidates. Their versatility allows for a wide range of possible combinations, making them highly adaptable for various applications. Careful selection of precursors for the Schiff base synthesis enables precise control over the cavities [20,28], the denticity of the ligand [29,30], the charge of the deprotonated ligand [15,31], the nature of the donor atoms [29,32], and even the distance between metallic centers [33]. This control enables the design of these ligands for specific purposes.

Diamines have been commonly used as precursors for synthesizing Schiff bases through condensation with suitable ketones or aldehydes in coordination chemistry [34–39]. In comparison, using oxalyl dihydrazide as a building block for Schiff bases introduces four additional donor atoms: two nitrogen and two oxygen atoms. This increase in donor atoms may enhance the coordination ability of the Schiff base, potentially resulting in a greater number of cations within the complex.

The aim of this study was twofold: first, to conduct preliminary experiments with three oxalyl dihydrazide-derived Schiff bases complexed with 3d metals, providing insight into the coordination behavior of these ligands; and second, to explore their magnetic properties in order to assess their potential for future applications in magnetic materials.

Oxalyl dihydrazide was condensed with pyridine derivatives such as 2-pyridylcarboxyaldehyde, 2-benzoylpyridine, and 6-methylpyridine-2-carboxaldehyde to obtain N′1,N′2-bis((*E*)-pyridin-2-ylmethylene)oxalohydrazide (**$H_2$L1**), N′1-((*E*)-(3-methylpyridin-2-yl)methylene)-N′2-((*E*)-(6-methylpyridin-2-yl)methylene)oxalohydrazide (**$H_2$L2**), and N′1,N′2-bis((E)-phenyl(pyridin-2-yl)methylene)oxalohydrazide (**$H_2$L3**), respectively (Figure 1).

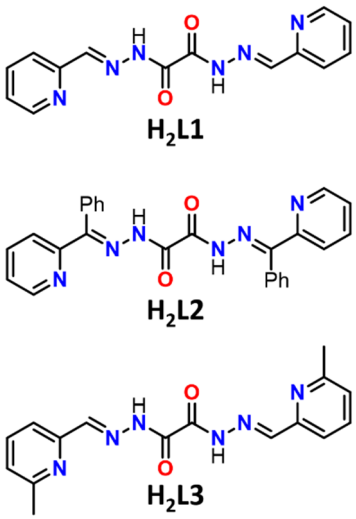


**Figure 1.** Oxalyl-derived ligands employed in this work.

Then, a series of preparations were conducted, during which various parameters, primarily structural ones, were modified to assess their impact on the magnetic properties. As is well known, ligands, metal ions, and counter ions play essential roles in determining the geometry and structure of a complex. Ligands stabilize specific geometries, while the size, charge, and electronic configuration of metal ions influence the overall structure. Additionally, counter ions impact solubility and crystallinity, which, in turn, can affect the compound's final structure.

Therefore, the combination of these ligands with various Mn(II), Ni(II), and Cu(II) salts resulted in the formation of corresponding metal complexes, such as $[Cu_5(L1)_2(H_2O)_8(MeOH)_2(NO_3)_2](NO_3)_4$ (**1**), $[Mn_2(HL2)_2(BzO)_2(MeOH)_2]\cdot 2MeOH$ (**2**), $[Ni(HL2)_2]\cdot 2MeOH$ (**3**), $[Ni_4(L2)_4]\cdot 4MeOH$ (**4**), and $[Ni_8(L3)_4(AcO)_4(H_2O)_{12}](OAc)_4$ (**5**), evidencing the various

coordination modes that these ligands can adopt (Figure 2) and the self-assembly for Ni(II) compounds **4** and **5**. Direct current susceptibility ($\chi_M T$) measurements were conducted for compounds **1**, **2**, **4**, and **5** and then were analyzed to determine the superexchange coupling between the metal centers. Susceptibility measurements for compound **3** were not conducted, as it is a mononuclear Ni(II) complex for which Curie-law behavior is expected. Temperature and frequency variable alternate current (*ac*) measurements were performed for **1**, evidencing no slow relaxation of the magnetization.

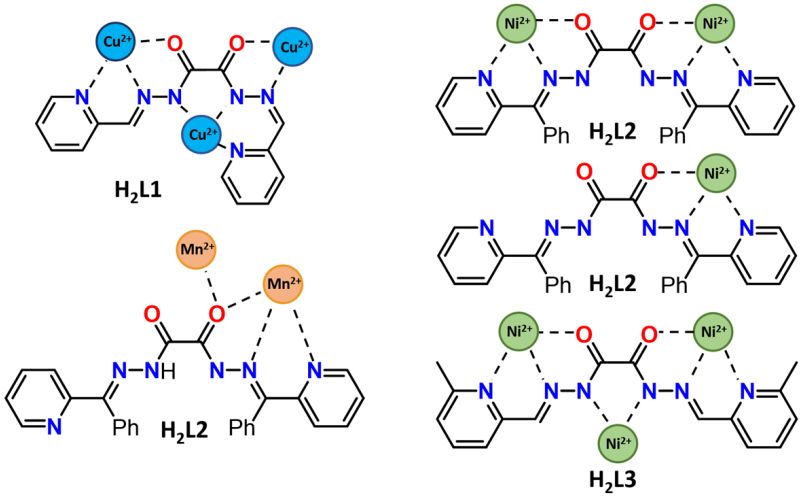


**Figure 2.** Coordination modes observed for $\mathbf{H_2L1}$, $\mathbf{H_2L2}$, and $\mathbf{H_2L3}$ ligands.

## 2. Materials and Methods

### *2.1. X-Ray Crystallography*

Single crystal X-ray diffraction measurements were performed with a D8 Venture system equipped with a multilayer monochromator and a Mo microfocus (λ = 0.71073 Å). The frames were integrated with the Bruker SAINT software package using a narrow-frame algorithm. The structures were solved and refined using the Bruker SHELXLE Software [40]. In most cases, hydrogen atoms were computationally modeled, with isotropic temperature factors assigned as 1.2 or 1.5 times the values of their corresponding bonded atoms. Crystal data and refinement details for complexes **1**–**5** are summarized in Table S1.

CCDC numbers: 2,390,280 (for **1**), 2,390,353 (for **2**) 2,390,354 (for **3**), 2,390,355 (for **4**), and 2,390,303 (for **5**) contain the supplementary crystallographic data for this paper. These data can be obtained free of charge via https://www.ccdc.cam.ac.uk/structures/ (accessed on 10 October 2024).

Powder X-ray diffraction was performed with a PANalytical X'Pert PRO MPD θ/θ powder diffractometer of 240 millimeters of radius in a configuration of convergent beam with a focalizing mirror and a transmission geometry with flat samples sandwiched between low-absorbing films and CuKα radiation (λ = 1.5418 Å).

### *2.2. Physical Measurements*

The elemental analyses of C, H, and N for compounds **1**–**6** were carried out at the Centres Científics i Tecnològics of the University of Barcelona.

Infrared spectra (4000–400 $cm^{-1}$) were recorded from KBr pellets on a Bruker IFS-125 FT-IR spectrophotometer.

Magnetic susceptibility measurements were carried out on pressed polycrystalline samples with an MPMS5 Quantum Design susceptometer working in the range of 30–300 K under magnetic fields of 0.3 T and a field of 0.03 T in the 30–2 K range to avoid any saturation effects at low temperature. Diamagnetic corrections were estimated from Pascal tables [41].

## 3. Results and Discussion

### *3.1. Structural Description*

#### 3.1.1. $[Cu_5(L1)_2(H_2O)_8(MeOH)_2(NO_3)_2](NO_3)_4$ (**1**)

A partially labeled plot of **1** is shown in Figure 3. Selected bond parameters and angles are summarized in Table S2. The molecular structure of compound **1** consists of a cationic pentanuclear Cu(II) complex adopting a Zeta-planar configuration, coordinated by two Schiff base $L1^{2-}$ ligands. The complex crystallizes in the triclinic P-1 space group, with four nitrate ions serving as counterions, where one of the nitrate anions is found in a disordered position.

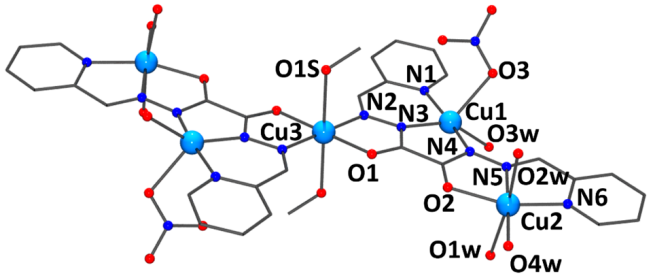


**Figure 3.** Partially labeled plot of **1**. Hydrogen atoms and non-coordinated nitrates have been omitted for clarity. Color code: Cu cyan, O red, N navy, and C grey.

Cu1 is pentacoordinated, while Cu2 and Cu3 cations are hexacoordinated. Cu1 has an $N_3O_2$ environment, coordinating with the ligand by N1, N3, and N4 with distances Cu1–N in the range of 1.943(3)–2.001(4) Å, one monodentate nitrato ligand, and one water molecule with distances Cu1–O of 2.017(3) and 2.014(3) Å. In the Cu1 coordination environment, the potential sixth coordination site involving the oxygen atom (O11B) from a disordered nitrate anion has been excluded from consideration as it is situated at a significant distance of 2.793(4) Å, which limits its relevance. $Cu_2$ has an $N_2O_4$ coordination environment, with the ligand binding through $N_5$, $N_6$, and $O_2$ and three water molecules that fill the remaining coordination sphere. $Cu_2$–N distances are 1.934(4) and 2.029(4) Å. $Cu_2$–O equatorial distances are 1.922(3) and 2.064(3) Å, while $Cu_2$–O axial distances are 2.422(5) and 2.444(4) Å, indicating a pronounced Jahn-Teller distortion. $Cu_3$ is located in the center of the pentanuclear molecule, serving as a bridge between the two asymmetrical units. It has an $N_2O_4$ environment coordinated to the ligand by N2 and O1 of both ligands and two MeOH molecules from the solvent. The distances $Cu_3$–N, $Cu_3$–O, and $Cu_3$–$O_{MeOH}$ are 1.964(3), 2.003(3), and 2.310(4) Å, respectively. A pronounced Jahn–Teller distortion is observed in $Cu_3$ as evidenced by the substantial difference between the $Cu_3$–O and $Cu_3$–$O_{MeOH}$ bond distances. All angles for $Cu_3$ are close to 90°, indicating low distortion around the metal. The nearest-neighbor Cu···Cu distances are 4.793(3), 4.707(3), and 6.746(3) Å.

SHAPE [42] calculations have been performed for all three Cu(II) cations, revealing a highly distorted coordination environment relative to ideal polyhedral geometries, being a trigonal bipyramid for Cu1, the closest one with a very large CShM value of 3.41. For Cu2 and Cu3, the octahedron was found to be the closest polyhedron to their coordination environment with CShM values of 2.06 and 0.95, respectively (Table S7 and Figure S1).

#### 3.1.2. $[Mn_2(HL2)_2(BzO)_2(MeOH)_2]\cdot 2MeOH$ (**2**)

A partially labeled plot of **2** is shown in Figure 4. Selected bond parameters and angles are summarized in Table S3. The molecular structure of **2** consists of a neutral dinuclear complex of $Mn^{II}$ and two partially deprotonated ligands ($HL2^-$), two benzoate

co-ligands, and two MeOH molecules that crystallize in the P-1 triclinic system. Both $Mn^{II}$ are structurally equivalent due to the existence of an inversion center.

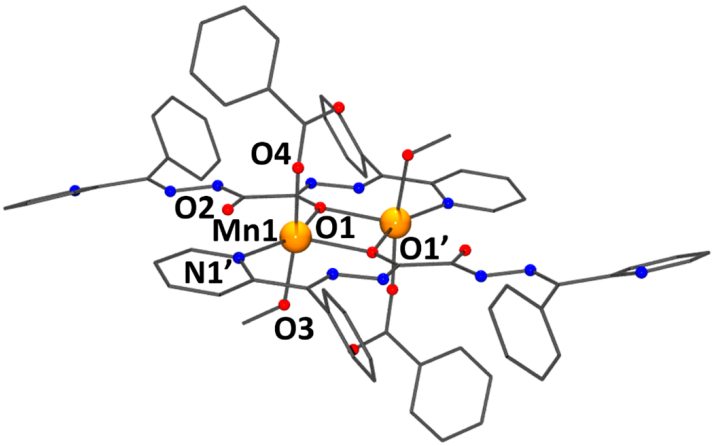


**Figure 4.** Partially labeled plot of **2**. Hydrogen atoms have been omitted for clarity. Color code: Mn orange, O red, N navy, and C grey.

Mn1 can be hexacoordinated with an $N_2O_4$ environment or heptacoordinated with an $N_2O_5$ environment. It is coordinated to the ligand through N1, N2, O1, and O1′ with distances Mn1–N of 2.281(1) and 2.320(2) Å and Mn1–O of 2.169(1) and 2.216(1) Å. A benzoate co-ligand, acting as a monodentate, and a MeOH molecule are bonded to the Mn1 to fulfill the coordination sphere with Mn1–O distances of 2.096(2) and 2.216(1) Å. If one considers the Mn1–O2 bond length of 2.572(2) Å as a coordination bond, it suggests that $Mn^{II}$ is in a heptacoordination environment, characterized by a distinctly different geometry. The nearest-neighbor Mn···Mn distance is 3.625(4) Å, and the Mn–O–Mn angle is 111.53°.

SHAPE [42] calculations have been performed for the Mn1 cation considering both possible coordination geometries. For hexacoordinated Mn1, a very distorted environment with respect to any polyhedron was obtained, being a trigonal prism, the closest one with an extremely large CShM value of 6.26 (Table S8 and Figure S2). Such a degree of distortion is due to the omission of the $Mn^{II}$–O2 bond since a distance of 2.572(2) Å is observed.

When considering the above-mentioned $Mn^{II}$–O2 bond as a real coordination bond, a heptacoordination environment for $Mn^{II}$ is observed. The distortion with respect to any polyhedron has been calculated as being a pentagonal bipyramid, the closest one with a CShM value of 1.50 (Table S8 and Figure S2). Due to this value, despite the Mn–O2 bond distance, the heptacoordinated environment should be considered the real for both Mn cations.

#### 3.1.3. $[Ni(HL2)_2]\cdot 2MeOH$ (**3**)

A partially labeled plot of **3** is shown in Figure 5. Selected bond parameters and angles are listed in Table S4. The molecular structure of **3** consists of a neutral mononuclear compound of hexacoordinated $Ni^{II}$ cation, two partially deprotonated ligands ($HL2^-$), and two MeOH molecules, which crystallize in the P-1 triclinic system. The $Ni^{II}$ cation is hexacoordinated with an $N_4O_2$ environment. Ni1–N distances are comprised between 1.986(18) and 2.104(2) Å, and Ni1–O distances are 2.101(16) for O1 and 2.077(16) for O3. The N–Ni1–N angles are 78.38(7)° for N1–Ni1–N2 and 78.72(8)° for N7–Ni1–N8, which are slightly lower in value for an ideal octahedron.

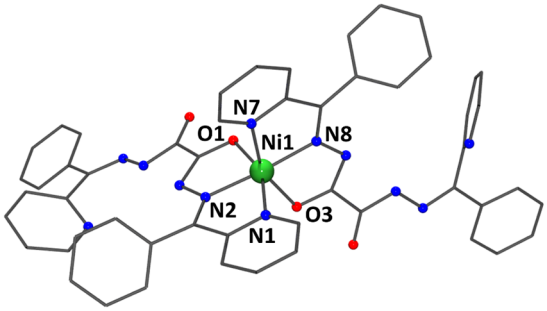


**Figure 5.** Partially labeled plot of **3**. Hydrogen atoms have been omitted for clarity. Color code: Ni green, O red, N navy, and C grey.

SHAPE [42] calculations have been performed for the Ni1 cation, indicating a very distorted environment with respect to any polyhedron, being an octahedron the closest one with a very large CShM value of 3.20 for Ni1 (Table S9 and Figure S3). This level of distortion in the Ni cation can be attributed to the small angles of the N–Ni–N bonds.

3.1.4. $[Ni_4(L2)_4]\cdot 4MeOH$ (**4**)

A plot of **4** is shown in Figure 6a along with the partially labeled plot of the core of the molecule (Figure 6b). Selected bond parameters and angles are summarized in Table S5. The molecular structure of **4** consists of a neutral [2 × 2] grid of four $Ni^{II}$ cations and four fully deprotonated ligands ($L2^{2-}$) that crystallize in the P21/n monoclinic system. The four $Ni^{II}$ cations are hexacoordinated with an $N_4O_2$ environment. To avoid repetition, only the $Ni^{II}$ cations in the asymmetric unit will be described. Ni1–N distances are comprised between 1.997(6) and 2.083(7) Å, and Ni1–O distances are 2.103(5) and 2.141(5). For Ni2, the distances Ni1–N are in the range of 1.984(7)–2.059(7) Å, while Ni2–O are slightly larger, with distances Ni2–O3 and Ni2–O2 of 2.099(5) and 2.104(5) Å, respectively. The N–Ni1–N angles are 77.67(7)° and 78.07(3)° for N1–Ni1–N2 and N11–Ni1–N12, respectively. For Ni2, the N–Ni2–N angles are 77.41(3)° for N5–Ni2–N6 and 77.94(3)° for N7–Ni2–N8, which are, in both cases, slightly lower in value for an ideal octahedron. The nearest-neighbor Ni···Ni distances are quite similar, being 6.861(2) and 6.913(2) Å.

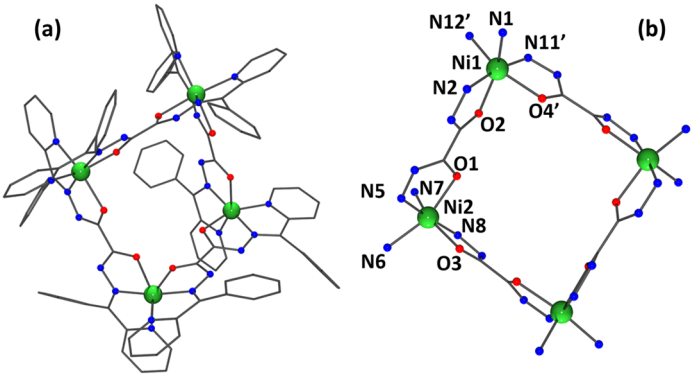


**Figure 6.** (**a**) Structural representation of complex **4**. (**b**) Partially labeled plot of **4**. Hydrogen and atoms that are not part of the coordination sphere of the metals have been omitted for clarity. Color code: Ni green, O red, N navy, and C grey.

SHAPE [42] calculations have been performed for both Ni1 and Ni2 cations, indicating a very distorted environment with respect to any polyhedron, being an octahedron the closest one with a very large CShM value of 3.48 for Ni1 and 3.11 for Ni2, respectively (Table S10 and Figure S4). Such a degree of distortion for both Ni cations can be attributed to the small N–Ni–N angle.

3.1.5. $[Ni_8(L3)_4(AcO)_4(H_2O)_{12}](OAc)_4$ (**5**)

A plot of compound **5** is shown in Figure 7a along with the partially labeled plot of the core of the molecule (Figure 7b). Selected bond parameters and angles are summarized in Table S6. The molecular structure of **5** consists of a cationic octanuclear ring of hexacoordinated $Ni^{II}$ cations, four fully deprotonated ligands ($L3^{2-}$), four coordinating acetates, and four more acetates acting as counter anions, which crystallize in the I41/a tetragonal system.

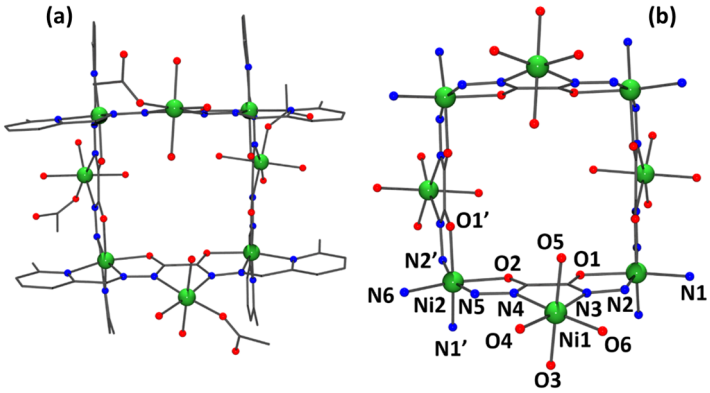


**Figure 7.** (**a**) Cationic structure representation of **5**. (**b**) Partially labeled plot of **5**. Hydrogen atoms and part of acetate anions have been omitted for clarity. Color code: $Ni^{II}$ green, O red, N navy, and C grey.

Ni1 is positioned within the ligand's structure, precisely at a site that does not involve the oxygen atoms. It has an $N_2O_4$ environment coordinated to the ligand by N3 and N4 with distances of 2.075(6) and 2.101(5) Å, respectively. To complete the coordination sphere, three water molecules, and a monodentate acetate ligand are bonded to Ni1 with distances Ni–O varying between 2.032(5) and 2.098(7) Å. The N1–Ni1–N2 angle value is 78.07(2)° and the N5–Ni1–N6 is 78.26(2)°, conferring to the cation significant distortion. Ni2 is situated on the side of the ligand that incorporates the oxygen atoms. It has a $N_3O_3$ environment coordinated to the ligand by N1, N2 and O1 with distances of 2.134(5), 1.993(6) and 2.093(4) Å, respectively. Ni2 serves as a bridge to the neighboring asymmetric unit by coordinating with N5 and O2, with bond distances of 1.981(6) Å and 2.087(4) Å, respectively. Ni1 and Ni2 of the same asymmetric unit are bonded through the N4–N5 diaza bridge, defining a dihedral angle of 166.6(4)°, while the dihedral angle between the Ni1 and the Ni2 cations from the other neighboring asymmetric unit, connected by the N2–N3 bridge, is 176.2(3)°. The Ni···Ni intermetallic distances are quite similar on the side of the diaza fragment, with values of 4.981(2) Å and 4.966(2) Å for the Ni1···Ni2 and Ni2···Ni1′, respectively, while it is different through the oxalyl group, being 6.822(2) Å for Ni(2)···Ni(2)′′.

SHAPE [42] calculations have been performed for both Ni1 and Ni2 cations, indicating a very distorted environment for Ni2 with respect to any polyhedron, being an octahedron the closest one with a very large CShM value of 0.48 for Ni1 and 3.72 for Ni2. (Table S11 and Figure S5). The degree of distortion observed for both Ni cations can be attributed to the low N–Ni–N angle, correlating the higher CShM value to the Ni containing two N–Ni–N angles.

### *3.2. Magnetic Properties*

Static Measurements

Magnetic susceptibility was measured on polycrystalline samples within the temperature range of 2–300 K for compounds **1**, **2**, **4**, and **5**. The phase purity of the complexes

was confirmed by the PXRD pattern (Figure S6). However, for complex **5**, the experimental PXRD pattern shows a slight deviation from the simulated one, which may be due to partial loss of the crystallization solvents. This, however, does not impact the magnetic properties of the compound. The results are depicted in Figure 8a as $\chi_M T$ vs. *T*. At room temperature, $\chi_M T$ of **1** shows a value of 1.783 $cm^3$ $mol^{-1}$ K for the pentanuclear unit, close to that expected for five uncoupled $S = 1/2$ ions with $g = 2.0$ (1.875 $cm^3$ $mol^{-1}$ K). On cooling, $\chi_M T$ decreases quickly, showing a plateau from ca. 25 K with a $\chi_M T$ value of ca. 0.431 $cm^3$ $mol^{-1}$ K. This suggests a moderate antiferromagnetic coupling for compound **1**. For compounds **2** and **4**, the values of $\chi_M T$ are 8.871 $cm^3$ $mol^{-1}$ K and 4.195 $cm^3$ $mol^{-1}$ K, respectively. These values are in good agreement with those expected at 300 K (8.75 and 4.00 $cm^3$ $mol^{-1}$ K for a dinuclear Mn(II) and a tetranuclear Ni(II) uncoupled compound, respectively, assuming $g = 2.00$). Upon cooling, the $\chi_M T$ values remain nearly constant down to 80 K for compound **2** (8.298 $cm^3$ $mol^{-1}$ K) and down to 50 K for compound **4** (4.083 $cm^3$ $mol^{-1}$ K). Below these temperatures, the $\chi_M T$ values decrease sharply, reaching 1.499 $cm^3$ $mol^{-1}$ K for compound **2** and 2.268 $cm^3$ $mol^{-1}$ K for compound **4** at 2 K. This sharp decline suggests very weak magnetic coupling in both compounds. In the case of compound **5**, $\chi_M T$ measures 8.023 $cm^3$ $mol^{-1}$ K at 300 K, in accordance with the expected value of eight isolated $S = 1$ ions with $g = 2.0$ (8.00 $cm^3$ $mol^{-1}$ K). As the temperature decreases, the $\chi_M T$ value gradually declines, reaching 0.208 $cm^3$ $mol^{-1}$ K at 2 K, which is close to the anticipated value of zero for an octanuclear Ni(II) coupled antiferromagnetically.

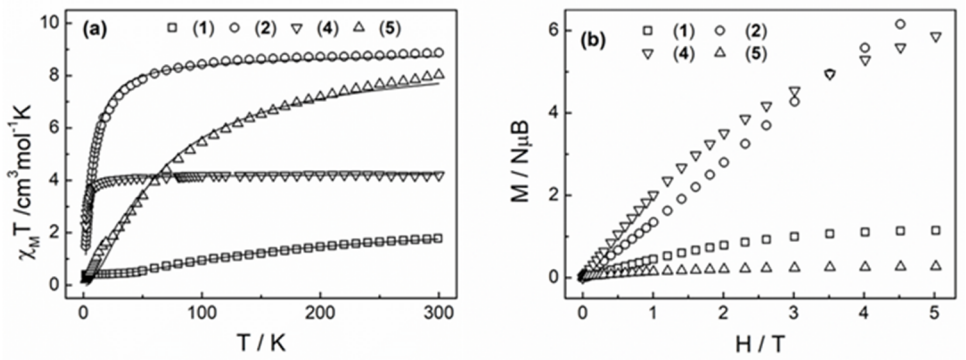


**Figure 8.** (**a**) Plots of $\chi_M T$ vs. *T* and (**b**) reduced magnetization vs. *H* for compounds **1**, **2**, **4**, and **5**. The open points are the experimental ones and the solid lines correspond to the best fit obtained.

To quantify the magnetic behavior, the experimental data were fitted using the *Phi* program [43] to resolve the considered spin-only Hamiltonians $H_1$–$H_4$ of Equations (1)–(4). These Hamiltonians describe the different considered magnetic interactions between the metal centers in each compound, as illustrated in Scheme 1. The *g* values were assumed to be isotropic and uniform across all the metal ions. The best-fit parameters obtained for compounds **1**, **2**, **4**, and **5** are summarized in Table 1.

$$H_1 = -2J_1(S_1 \cdot S_2 + S_1 \cdot S_3 + S_3 \cdot S_5 + S_5 \cdot S_4) - 2J_2(S_2 \cdot S_3 + S_3 \cdot S_4) \quad (1)$$

$$H_2 = -2J_1(S_1 \cdot S_2) \quad (2)$$

$$H_3 = -2J_1(S_1 \cdot S_2 + S_2 \cdot S_3 + S_3 \cdot S_4 + S_4 \cdot S_1) \quad (3)$$

$$H_4 = -2J_1(S_1 \cdot S_2 + S_2 \cdot S_3 + S_3 \cdot S_4 + S_4 \cdot S_5 + S_5 \cdot S_6 + S_6 \cdot S_7 + S_7 \cdot S_8 + S_8 \cdot S_1) - 2J_2(S_1 \cdot S_3 + S_3 \cdot S_5 + S_5 \cdot S_7 + S_7 \cdot S_1) \quad (4)$$

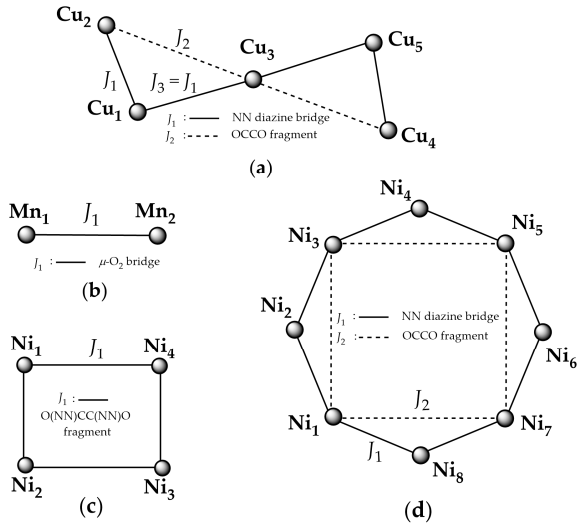


**Scheme 1.** Schematic diagram representing the exchange interactions within (**a**) for **1**, (**b**) for **2**, (**c**) for **4**, and (**d**) for **5**. The magnetic interaction $J_2$ has been regarded as negligible and only $J_1$ has been considered for **1** and **5**. For **1**, $J_3$ was assumed equal to $J_1$.

**Table 1.** Best fit parameters for compounds **1**, **2**, **4**, and **5**.

| Compound | $2J_1$ ($cm^{-1}$) | $g$ | $R$ [1] |
|---|---|---|---|
| **1** | $-60.87 \pm 0.01$ | 2.09 | $4.70 \times 10^{-4}$ |
| **2** | $-0.47 \pm 0.01$ | 2.00 | $7.20 \times 10^{-4}$ |
| **4** | $-0.23 \pm 0.01$ | 2.06 | $6.71 \times 10^{-5}$ |
| **5** | $-11.50 \pm 0.19$ | 2.13 | $2.57 \times 10^{-3}$ |

[1] The error, $R$ due to the divergence between the experimental and calculated data for the different fits was determined using the following equation $R = \frac{\sum(\chi_M T_{exp} - \chi_M T_{cal})^2}{\sum \chi_M T_{exp}{}^2}$.

It is important to note that in the case of 1, only a single superexchange interaction was taken into account, assuming that $J_3 = J_1$ as illustrated in Scheme 1a, and $J_2$ superexchange interaction was considered negligible. For compound **5**, in addition to assuming $J_2 = 0$, a parameter representing the possible presence of a monomeric impurity, ρ, was introduced in the fit process, with a value of $0.204 \times 10^{-4}$.

The antiferromagnetic behavior observed in **1**, **2**, **4**, and **5** was confirmed by magnetization measurements performed at 2 K, up to an external field of 5 T (Figure 8b). At higher fields, the reduced molar magnetization, $M/N\mu B$, tends to 1.14 NμB for **1**, aligning well with the expected one effective electron for a [$Cu_5$] system antiferromagnetically coupled. In contrast, compounds **2** and **4** reach maximum reduced molar magnetization values of 6.68 NμB and 5.86 NμB, respectively. These values are lower than expected for non-coupled [$Mn_2$] (ten effective electrons) and [$Ni_4$] (eight effective electrons) systems, suggesting that both compounds exhibit weak antiferromagnetic coupling. For compound **5**, the reduced magnetization, $M/N\mu B$, shows a continuous increase in the magnetization, achieving a value of only 0.27 NμB at 5T. Such a value is near the expected value for an antiferromagnetically coupled [$Ni_8$] (zero effective electrons) system, indicating diamagnetic behavior at 2 K.

The super-exchange parameters for complexes **1**, **2**, **4**, and **5** can be correlated with the nature of the bridging interactions between the Cu(II), Mn(II), and Ni(II) ions, which are mainly influenced by the inter-metallic connections within the oxalohydrazide ligand spacer in complexes **1**, **4**, and **5** and double alkoxo group in complex **2** (Figure 2). The arrangement of the metal centers is governed by the ligand's conformational flexibility,

allowing it to adapt and effectively coordinate with the metal ions. This structural adaptation subsequently impacts the strength and nature of the exchange coupling. Notably, the key factor driving antiferromagnetic coupling is the degree of overlap between the metal magnetic orbitals and the p orbitals on the nitrogen atoms of the N–N diazine bridge group (in **1** and **5**).

For compound **1**, each pair of adjacent Cu(II) centers is bridged by an N–N diazine group in a trans fashion, showing high torsion angles (τ) of 166.9° and 175.1°, a factor that weakens the degree of overlap. With this, a moderate value of magnetic interaction is expected, in contrast to the strong antiferromagnetic interactions observed in N–N diazine Cu(II) systems with smaller torsion angles [44].

In the dinuclear Mn(II) compound (**2**), the magnetic interaction is mediated through the double alkoxo bridge, unlike the other compounds, where it is influenced by several structural parameters, such as the Mn–O–Mn bond angle (θ), Mn···Mn and Mn–O distances, and the torsion angle (τ). Therefore, the obtained magnetic parameter, $2J = -0.47$ cm$^{-1}$, results from the combined effect of these structural factors: the Mn–O–Mn angle (111.35°), Mn···Mn distance (3.625 Å), Mn-O distances (2.166 and 2.206 Å), and the torsion angle (τ = 0). The absolute value of the exchange parameter obtained, along with these structural parameters, closely matches those found in other alkoxo/phenoxo-bridged dinuclear Mn(II) complexes, as reported in the article by V. Gómez et al. [45].

For the Ni(II) complexes **4** and **5**, the linkage between the Ni(II) ions differs significantly. In complex **4**, considering the compound's topology (with a slight distortion from a square planar arrangement), the Ni(II) ions are bridged end-to-end by the oxalohydrazide ligand (O(NN)CC(NN)O fragment, see Figure 2). The Ni(II) ions are separated by distances of 6.913 Å and 6.861 Å, which are long for any significant magnetic exchange between the metal centers, and no cross-coupling connection is appreciated. Furthermore, the oxalohydrazide is twisted around the C–C bond, displaying a torsion of 22.94°, which further hinders the potential for magnetic exchange. These factors are clearly reflected in the magnetic data, with $2J = -0.23$ cm$^{-1}$ [46]. In contrast, the Ni(II) atoms in complex **5** are bridged (I) by an end-to-end connection involving the O–C–C–O fragment of the oxalohydrazide ligand (6.822 Å) and (II) by the N–N diazine group of the same ligand (with inter-metallic distances of 4.966 Å and 4.981 Å), as shown in Figure 2. The torsion around the C–C bond does not exceed 1.67°. These factors suggest a more favorable magnetic exchange interaction compared to complex **4**, as supported by the experimental data, which show a $2J$ value of $-11.50$ cm$^{-1}$. This value closely aligns with the octanuclear Ni(II) compound $Ni_8(DPKOH\text{-}2H)_4(H_2O)_8(BF4)_8 \cdot 16H_2O$, reported by L.K. Thompson [47].

## 4. Experimental Section

Oxalyldihydrazide, 2-pyridylcarboxyaldehyde, 2-benzoylpyridine, 6-methylpyridine-2-car-boxaldehyde, Cu, and Ni salts were used as they were purchased. $Mn(BzO)_2$ and $Ni(BzO)_2$ were synthesized following a previously reported procedure [48]. High-pressure reactions were performed in a Microwave Synthesis Reactor Anton Paar Monowave 300.

### *4.1. Synthesis of the Ligands*

The ligands were synthesized following the reported method [49].

#### 4.1.1. Synthesis of $\mathbf{H_2L1}$

The ligand $\mathbf{H_2L1}$ was synthesized by a reaction of oxalyldihydrazide (0.295 g, 2.5 mmol) dissolved in 25 mL of $H_2O$ with 2-pyridylcarboxyaldehyde (0.532 g, 5 mmol) in 12.5 mL of MeOH. Both solutions are mixed and refluxed under continuous stirring for 20 h to achieve a better yield (80%), then the white precipitate of N′1,N′2-bis((*E*)-

pyridin-2-ylmethylene)oxalohydrazide (**$H_2$L1**) was filtered, washed with methanol as dried in vacuum.

#### 4.1.2. Synthesis of **$H_2$L2** and **$H_2$L3**

The same procedure was used for **$H_2$L2** and **$H_2$L3**. 2-benzoylpyridine (0.916 g, 5.0 mmol) and 6-methylpyridine-2-carboxaldehyde (0.604 g, 5.0 mmol) were dissolved respectively in 12.5 mL of MeOH. Each solution is mixed with the corresponding solution of oxalyl dihydrazide. Then refluxed under continuous stirring during aporox. 20 h. The white precipitate formed was filtered, washed with methanol, and dried in a vacuum to obtain N′2-((*E*)-phenyl(pyridin-2-yl)methylene)-N′1-((*Z*)-phenyl(pyridin-2-yl)methylene) oxalohydrazide (**$H_2$L2**) and N′1,N′2-bis((*E*)-(6-methylpyridin-2-yl)methylene)oxalohydrazide (**$H_2$L3**) with yields of 74% and 77%, respectively.

### *4.2. Synthesis of the Complexes*

#### 4.2.1. Synthesis of $[Cu_5(L1)_2(H_2O)_8(MeOH)_2(NO_3)_2](NO_3)_4$ (**1**)

A suspension solution of $H_2$L1 (0.074 g, 0.25 mmol) was added to 20 mL of methanolic solution of $Cu(NO_3)_2{\cdot}3H_2O$ (0.234 g, 1.25 mmol). The mixture suspension was stirred at room temperature for 2 h. The resulting solution was kept under stirring for a further 2 h. Then filtered and slowly evaporated. $[Cu_5(L1)_2(H_2O)_8(MeOH)_2(NO_3)_2](NO_3)_4$ (**1**) was obtained as plate-like dark green crystals suitable for X-ray diffraction in the period of a week in 60% of yield.

#### 4.2.2. Synthesis of $[Mn_2(HL2)_2(BzO)_2(MeOH)_2]{\cdot}2MeOH$ (**2**)

$H_2$L2 (0.069 g, 0.15 mmol) and $Mn(BzO)_2$ (0.069 g, 0.25 mmol) were added to a microwave furnace vial along with 20 mL of MeOH. The reaction was heated and stirred for 30 min at 80 °C. The resulting orange solution was filtered. Then slowly diffused with $Et_2O$. $[Mn_2(HL2)_2(BzO)_2(MeOH)_2]{\cdot}2MeOH$ (**2**) was obtained as prism-like orange crystals suitable for X-ray diffraction in the period of 2 days in 45% of yield.

#### 4.2.3. Synthesis of $[Ni(HL2)_2]{\cdot}2MeOH$ (**3**)

$H_2$L2 (0.134 g, 0.30 mmol) and $Ni(BzO)_2$ (0.027 g, 0.15 mmol) were added to microwave furnace vials along with 20 mL of MeOH. The reaction was heated and stirred for 30 min at 80 °C. The resulting orange solution was filtered. Then slowly evaporated. $[Ni(HL2)_2]{\cdot}2MeOH$ (**3**) was obtained as prism-like red crystals suitable for X-ray diffraction in the period of 5 days in 40% of yield.

#### 4.2.4. Synthesis of $[Ni_4(L2)_4]{\cdot}4MeOH$ (**4**)

$H_2$L2 (0.066 g, 0.15 mmol) and $Ni(NO_3)_2{\cdot}5H_2O$ (0.048 g, 0.15 mmol) were added to microwave furnace vials along with 20 mL of MeOH. The reaction was heated and stirred for 30 min at 80 °C. The resulting orange solution was filtered. Then slowly evaporated. $[Ni_4(L2)_4]{\cdot}4MeOH$ (**4**) was obtained as prism-like red crystals suitable for X-ray diffraction in the period of 2 days in 30% of yield.

#### 4.2.5. Synthesis of $[Ni_8(L3)_4(AcO)_4(H_2O)_{12}](OAc)_4$ (**5**)

A solution of $Ni(OAc)_2$ (0.369 g, 1.5 mmol) in 10 mL of MeOH was added to a solution of $H_2$L3 (0.125 g, 0.4 mmol) in 10 mL of MeOH. The solution was stirred for a further hour, filtered, and layered in $Et_2O$. One week later, $[Ni_8(L3)_4(AcO)_4(H_2O)_{12}](OAc)_4$ (**5**) was obtained as prism-like red crystals suitable for X-ray diffraction in 70% of yield.

Elemental analyses of C, H, and N and the most relevant IR bands, [50] of compounds **1**–**5** are reported below:

For **1**: Selected IR bands (KBr pellet, $cm^{-1}$): 3445 (s, $\upsilon_{(O–H)}$), 2920 (w, $\upsilon_{(–C–H)}$), 1569 (s, $\upsilon_{(C=O\ or\ C=N)}$), 1384 (s, $\upsilon_{(N–O)}$) from nitrate anions: $C_{30}H_{44}Cu_5N_{18}O_{32}$ (1485.98): Calc. (%) C 24.24, H 2.98, N 16.96; Found (%) C 24.3, H 2.7, N 16.7.

For **2**: Selected IR bands (KBr pellet, $cm^{-1}$): 3437 (s, $\upsilon_{(O–H)}$), 2989 (w, $\upsilon_{(–C–H)}$), 1572 (s, $\upsilon_{(C=O\ or\ C=N)}$). $C_{70}H_{64}Mn_2N_{12}O_{12}$ (1375.21): Calc. (%) C 61.13, H 4.69, N 12.22; Found (%) C 61.2, H 4.7 N 12.3.

For **3**: Selected IR bands (KBr pellet, $cm^{-1}$): 3452 (s, $\upsilon_{(O–H)}$), 2965 (w, $\upsilon_{(–C–H)}$), 1565 (s, $\upsilon_{(C=O\ or\ C=N)}$). $C_{54}H_{45}N_{12}NiO_{32}$ (1016.73): Calc. (%) C 45.27, H 3.17, N 11.73; Found (%) C 45.1, H 2.9 N 11.75.

For **4**: Selected IR bands (KBr pellet, $cm^{-1}$): 3443 (s, $\upsilon_{(O–H)}$), 2936 (w, $\upsilon_{(–C–H)}$), 1566 (s, $\upsilon_{(C=O\ or\ C=N)}$). $C_{108}H_{90}N_{24}Ni_4O_{11}$ (2135.88): Calc. (%) C 60.76, H 4.25, N 15.75; Found (%) C 60.1, H 4.0 N 15.9.

For **5**: Selected IR bands (KBr pellet, $cm^{-1}$): 3404 (s, $\upsilon_{(O–H)}$), 2922 (w, $\upsilon_{(–C–H)}$), 1550 (s, $\upsilon_{(C=O\ or\ C=N)}$), 1546 (s, $\upsilon_{(C=N)}$),1282 (s, $\upsilon_{(C–O)}$) from acetate anions. $C_{80}H_{104}N_{24}Ni_8O_{36}$ (2447.55): Calc. (%) C 39.26, H 4.28, N 13.74; Found (%) C 38.7, H 3.9 N 13.9.

It should be noted that the stretching band at 1569 $cm^{-1}$ approx. could correspond to either the C=N or C=O bond in **1**–**5**, as they overlap. The absence of an N–H stretching band indicates that deprotonation of the CONH group has occurred. Furthermore, the band at 3445 $cm^{-1}$ may correspond to the O–H stretch of either methanol or water.

Powder X-ray diffraction (PXRD) measurements were carried out at room temperature. A comparison between the experimental PXRD data and simulated patterns obtained from single-crystal X-ray analysis confirmed the bulk identity of the samples (Figure S6). All compounds demonstrated stability at room temperature, remaining unchanged for several months.

## 5. Conclusions

The design of polytopic ligands for the preparation of polymeric complexes depends on several factors, particularly the topological complexity of the ligand. Moreover, the individual coordinating components within the ligand display diverse behaviors when interacting with different metal ions. In this context, five novel coordination compounds featuring oxalyl dihydrazide-derived Schiff bases with various 3d metals (Mn(II), Ni(II), and Cu(II)) have been successfully synthesized and characterized. These ligands demonstrate remarkable versatility, as they lead to different nuclearities regardless of the initial stoichiometric ratios, as observed in complexes **1**, **2**, **3**, and **5**. Furthermore, by carefully selecting specific pyridine derivatives, steric effects can be fine-tuned, allowing for the modulation of nuclearity—either increasing or decreasing it—as evidenced in complexes **4** and **5**. According to the limited number of previously reported structures, self-assembly plays a crucial role in the behavior of both nickel and manganese complexes, leading to the formation of manganese derivatives as dinuclear complexes, while the nuclearity of nickel complexes varies depending on the ligand-to-metal ratio [46].

Magnetic measurement reveals antiferromagnetic coupling between the metals leading to a diamagnetic behavior at low temperatures for complexes **2**, **4**, and **5**, while for complex **1**, the $\chi_M T$ vs. $T$ plot indicates antiferromagnetic behavior but leading to an S = 1/2 ground state at low temperature. For **1**, AC susceptometry measurements further confirmed the absence of single-molecule magnet (SMM) behavior in this compound.

**Supplementary Materials:** The following supporting information can be downloaded at: https://www.mdpi.com/article/10.3390/magnetochemistry11010004/s1, Table S1: Crystallographic data of compound **1**–**5**; Table S2–S6: Selected bond lengths (Å) and angles (°) for compounds **1**–**5**, respectively; Tables S7–S11: Data of Continuous Shape Measures calculation of different metal ions in compounds **1**–**5** deviations from the different ideal polyhedra and related Figures S1–S5. Figure S6: Experimental and simulation Powder X-ray Diffraction (PXRD) patterns for compounds **1**, **2**, **4** and **5**.

**Author Contributions:** The manuscript was developed through the collaborative efforts of all authors. Individual contributions are outlined below, detailing the specific contributions made by each author: E.C.-V., synthesis, structural characterization of compounds **2**, **3**, and **4**, performance of the magnetic measurements, analysis of the results of magnetic studies of the compounds, and edition of part of the original and final draft. M.O. and P.S., synthesis and characterization of compounds **1** and **5** respectively. C.P. performance of single-crystal X-ray diffraction experiments and refinement of the crystal structure. M.S.E.F., design, and development of the general idea of research, supervision, and preparation-edition of the final version of the manuscript. All authors have read and agreed to the published version of the manuscript.

**Funding:** This work was supported by the Spanish Ministry of Science and Innovation (MICINN) Project PID2023-146166NB-I00.

**Institutional Review Board Statement:** Not applicable.

**Informed Consent Statement:** Not applicable.

**Data Availability Statement:** The data presented in this study are available in this article or Supplementary Material.

**Conflicts of Interest:** The authors declare no conflicts of interest.

## References

1. Sessoli, R.; Gatteschi, D.; Caneschi, A.; Movak, N.A. Magnetic bistability in a metal-ion cluster. *Nature* **1993**, *365*, 141–143. [CrossRef]
2. Singh, P.; Schlittenhardt, S.; Thakre, D.; Kushvaha, S.K.; Kumar, S.; Karnamkkott, H.S.; Ruben, M.; Ibrahim, M.; Banerjee, A.; Mondal, K.C. Exploration of Vanadium (IV)-Based Single-Ion Magnet Properties in Diphosphonate-Supported Mixed-Valent Polyoxovanadates. *Cryst. Growth Des.* **2022**, *22*, 5666–5679. [CrossRef]
3. Stamatatos, T.C.; Foguet-Albiol, D.; Lee, S.-C.; Stoumpos, C.C.; Raptopoulou, C.P.; Terzis, A.; Wernsdorfer, W.; Hill, S.O.; Perlepes, S.P.; Christou, G. "Switching On" the Properties of Single-Molecule Magnetism in Triangular Manganese(III) Complexes. *J. Am. Chem. Soc.* **2007**, *129*, 9484–9499. [CrossRef]
4. Terazzi, E.; Rogez, G.; Gallani, J.-L.; Donnio, B. Supramolecular Organization and Magnetic Properties of Mesogen-Hybridized Mixed-Valent Manganese Single Molecule Magnets $[Mn^{III}_8Mn^{IV}_4O_{12}(L_{x,y,z}\text{-CB})_{16}(H_2O)_4]$. *J. Am. Chem. Soc.* **2013**, *135*, 2708–2722. [CrossRef]
5. Mathonière, C.; Lin, H.-J.; Siretanu, D.; Clérac, R.; Smith, J.M. Photoinduced Single-Molecule Magnet Properties in a Four-Coordinate Iron(II) Spin Crossover Complex. *J. Am. Chem. Soc.* **2013**, *135*, 19083–19086. [CrossRef]
6. Cornia, A.; Mannini, M.; Sessoli, R.; Gatteschi, D. Propeller-Shaped Fe4 and Fe3M Molecular Nanomagnets: A Journey from Crystals to Addressable Single Molecules. *Eur. J. Inorg. Chem.* **2019**, *2019*, 552–568. [CrossRef]
7. Novikov, V.V.; Pavlov, A.A.; Nelyubina, Y.V.; Boulon, M.-E.; Varzatskii, O.A.; Voloshin, Y.Z.; Winpenny, R.E.P. A Trigonal Prismatic Mononuclear Cobalt(II) Complex Showing Single-Molecule Magnet Behavior. *J. Am. Chem. Soc.* **2015**, *137*, 9792–9795. [CrossRef]
8. Dimakopoulou, F.; Efthymiou, C.G.; O'Malley, C.; Kourtellaris, A.; Moushi, E.; Tasiopooulos, A.; Perlepes, S.P.; McArdle, P.; Costa-Villén, E.; Mayans, J.; et al. Novel $Co_5$ and $Ni_4$ Metal Complexes and Ferromagnets by the Combination of 2-Pyridyl Oximes with Polycarboxylic Ligands. *Molecules* **2022**, *27*, 4701–4714. [CrossRef]
9. Maniaki, D.; Pilichos, E.; Perlepes, S.P. Coordination Clusters of 3d-Metals That Behave as Single-Molecule Magnets (SMMs): Synthetic Routes and Strategies. *Front. Chem.* **2018**, *6*, 461. [CrossRef]
10. Serra, J.; Font-Bardia, M.; Escuer, A.; Mayans, J. Slow Magnetic Relaxation in Silver(II) Macrocyclic Systems. *Inorg. Chem.* **2023**, *62*, 18804–18808. [CrossRef]
11. Yamada, Y.; Nakajima, H.; Kobayashi, C.; Shuku, Y.; Awaga, K.; Akine, S.; Tanaka, K. Synthesis of Isomeric $Tb^{3+}$-Phthalocyanine Double-Decker Complexes Depending on the Difference in the Direction of Coordination Plane and Their Magnetic Properties. *Chem. Eur. J.* **2023**, *29*, e202203272. [CrossRef] [PubMed]

12. Anwar, M.U.; Thompson, L.K.; Dawe, L.N.; Habib, F.; Murugesu, M. Predictable self-assembled [2 × 2] $Ln(III)_4$ square grids (Ln = Dy,Tb)—SMM behaviour in a new lanthanide cluster motif. *Chem. Commun.* **2012**, *48*, 4576–4578. [CrossRef] [PubMed]
13. Tubau, À.; Zinna, F.; Di Bari, L.; Font-Bardía, M.; Vicente, R. Luminescence, CPL and magnetic properties of 1D enantiopure Ln3+ complexes with (S-) and (R-) α-methoxyphenylacetate ligand. *Dalton Trans.* **2023**, *52*, 1122–1132. [CrossRef] [PubMed]
14. Evans, P.; Reta, D.; Whitehead, G.F.S.; Chilton, N.F.; Mills, D.P. Bis-Monophospholyl Dysprosium Cation Showing Magnetic Hysteresis at 48 K. *J. Am. Chem. Soc.* **2019**, *141*, 19935–19940. [CrossRef] [PubMed]
15. Costa-Villén, E.; Font-Bardia, M.; Mayans, J.; Escuer, A. Field-Induced Slow Relaxation of the Magnetization in Two Families of $[M^{II}Ln^{III}]$ Complexes. *Cryst. Growth Des.* **2024**, *24*, 5806–5817. [CrossRef]
16. Baskar, V.; Gopal, K.; Helliwell, M.; Tuna, F.; Wernsdorfer, W.; Winpenny, R.E.P. 3d–4f Clusters with large spin ground states and SMM behavior. *Dalton Trans.* **2010**, *39*, 4747–4750. [CrossRef]
17. Patrascu, A.A.; Briganti, M.; Soriano, S.; Calancea, S.; Allão Cassaro, R.A.; Totti, F.; Vaz, M.G.F.; Andruh, M. SMM Behavior Tuned by an Exchange Coupling LEGO Approach for Chimeric Compounds: First 2p–3d–4f Heterotrispin Complexes with Different Metal Ions Bridged by One Aminoxyl Group *Inorg. Chem.* **2019**, *58*, 13090–13101. [CrossRef]
18. Polyzou, C.D.; Efthymiou, C.G.; Escuer, A.; Cunha-Silva, L.; Papatriantafyllopoulou, C.; Perlepes, S.P. In search of 3d/4f-metal single-molecule magnets: Nickel (II)/lanthanide (III) coordination clusters. *Pure Appl. Chem.* **2013**, *85*, 315–327. [CrossRef]
19. Schmidt, S.F.M.; Merkel, M.P.; Kostakis, G.E.; Buth, G.; Ansona, C.E.; Powell, A.K. SMM behaviour and magnetocaloric effect in heterometallic 3d–4f coordination clusters with high azide: Metal ratios. *Dalton Trans.* **2017**, *46*, 15661–15665. [CrossRef]
20. Caballero, S.; Pilichos, E.; Font-Bardia, M.; Mayans, J.; Escuer, A. Field-Induced Slow Magnetic Relaxation in a New Family of Tetranuclear Double-Stranded $Cu_2^{II}$–$Ln_2^{III}$ Metallohelicates. *Cryst. Growth Des.* **2023**, *23*, 3711–3719. [CrossRef]
21. Singh, S.K.; Cramer, C.J.; Gagliardi, L. Correlating Electronic Structure and Magnetic Anisotropy in Actinide Complexes $[An(COT)_2]$, $An^{III/IV}$ = U, Np, and Pu. *Inorg. Chem.* **2020**, *59*, 6815–6825. [CrossRef] [PubMed]
22. Chatelain, L.; Walsh, J.P.S.; Pécaut, J.; Tuna, F.; Mazzanti, M. Self-Assembly of a 3d–5f Trinuclear Single-Molecule Magnet from a Pentavalent Uranyl Complex. *Angew. Chem.* **2014**, *126*, 13652–13656. [CrossRef]
23. Coronado, E. Molecular magnetism: From chemical design to spin control in molecules, materials and devices. *Nat. Rev. Mater.* **2020**, *5*, 87–104. [CrossRef]
24. Chicco, S.; Chiesa, A.; Allodi, G.; Garlatti, E.; Atzori, M.; Sorace, L.; De Renzi, R.; Sessoli, R.; Carretta, S. Controlled coherent dynamics of [VO(TPP)], a prototype molecular nuclear qudit with an electronic ancilla. *Chem. Sci.* **2021**, *12*, 12046–12055. [CrossRef]
25. Aromí, G.; Aguilà, D.; Gàmez, P.; Luis, F.; Roubeau, O. Design of magnetic coordination complexes for quantum computing *Chem. Soc. Rev.* **2012**, *41*, 537–546. [CrossRef]
26. Rocha, A.R.; García-Suárez, V.M.; Bailey, S.W.; Lambert, C.J.; Ferrer, J.; Sanvito, S. Towards molecular spintronics. *Nat. Mater.* **2005**, *4*, 335–339. [CrossRef]
27. Coronado, E.; Yamashita, M. Molecular spintronics: The role of coordination chemistry. *Dalton Trans.* **2016**, *45*, 16553–16555. [CrossRef]
28. Weickmann, D.; Frey, W.; Plietker, B. Synchronizing Steric and Electronic Effects in $\{Ru^{II}(NNNN,P)\}$ Complexes: The Catalytic Dehydrative Alkylation of Anilines by Using Alcohols as a Case Study. *Chem. Eur. J.* **2013**, *19*, 2741–2748. [CrossRef]
29. Whiteoak, C.J.; Torres Martin de Rosales, R.; White, A.J.P.; Britovsek, G.J.P. Iron(II) Complexes with Tetradentate Bis(aminophenolate) Ligands: Synthesis and Characterization, Solution Behavior, and Reactivity with $O_2$. *Inorg. Chem.* **2010**, *49*, 11106–11117. [CrossRef]
30. Das, A.; Goswami, S.; Sen, R.; Ghosh, A. Inclusion of Ln(III) in the Complexes of Co(II) with a Mannich Base Ligand: Development of Atmospheric $CO_2$ Fixation and Enhancement of Catalytic Oxidase Activities. *Inorg. Chem.* **2019**, *58*, 5787–5798. [CrossRef]
31. Hazra, S.; Kuznetsov, M.L.; Fatima, M.; Guedes da Silva, C.; Pombeiro, A.J.L. $M^{II}\cdots$Cl Interaction Supported Heterometallic $\{Ni^{I}Sn^{II}\}\{Sn^{IV}\}$ and $\{Ni^{II}Sn^{II}\}\{Sn^{II}\}$ Complex Salts: Possibility of Ion-Pair-Assisted Tetrel Bonds. *Cryst. Growth Des.* **2022**, *22*, 341–355. [CrossRef]
32. Fernandes, R.R.; Lasri, J.; Kirillov, A.M.; Guedes da Silva, M.F.C.; da Silva, J.A.L.; Fraústo da Silva, J.J.R.; Pombeiro, A.J.L. New $Fe^{II}$ and $Cu^{II}$ Complexes Bearing Azathia Macrocycles—Catalyst Precursors for Mild Peroxidative Oxidation of Cyclohexane and 1-Phenylethanol. *Eur. J. Inorg. Chem.* **2011**, *25*, 3781–3790. [CrossRef]
33. Dasa, M.; Bhuniab, P.; Mukherjeec, A.; Costa-Villén, E.; Mayans, J.; Guha, P. Antiferromagnetic resorcinol bridged dinuclear square-planar copper (II) complexes: Syntheses, structural, spectroscopic and magnetic properties. *Inorg. Chim. Acta* **2024**, *569*, 122134–122140. [CrossRef]
34. Schoumacker, S.; Hamelin, O.; Pecaut, J.; Fontecave, M. Catalytic Asymmetric Sulfoxidation by Chiral Manganese Complexes: Acetylacetonate Anions as Chirality Switches. *Inorg. Chem.* **2003**, *42*, 8110–8116. [CrossRef] [PubMed]
35. Melville, J.N.; Bernhardt, P.V. Electrochemical Exploration of Active Cu-Based Atom Transfer Radical Polymerization Catalysis through Ligand Modification. *Inorg. Chem.* **2021**, *60*, 9709–9719. [CrossRef] [PubMed]

36. Pointillart, F.; Bernot, K.; Colas, J.; Sorace, L.; Sessoli, R. Rational enhancement of the coordination capability of Ru(III)(salen)-nitronyl nitroxide building block: A step towards 2p–3d–4d magnetic edifices. *Inorganica Chim. Acta* **2008**, *361*, 3427–3431. [CrossRef]
37. Senapati, T.; Pichon, C.; Ababei, R.; Mathoniere, C.; Clerac, R. Cyanido-Bridged Fe(III)–Mn(III) Heterobimetallic Materials Built From Mn(III) Schiff Base Complexes and Di- or Tri-Cyanido Fe(III) Precursors. *Inorg. Chem.* **2012**, *51*, 3796–3812. [CrossRef]
38. Maeda, M.; Hino, S.; Yamashita, K.; Kataoka, Y.; Nakano, M.; Yamamura, T.; Kajiwara, T. Correlation between slow magnetic relaxation and the coordination structures of a family of linear trinuclear Zn(II)–Ln(III)–Zn(II) complexes (Ln = Tb, Dy, Ho, Er, Tm and Yb). *Dalton Trans.* **2012**, *41*, 13640–13648. [CrossRef]
39. Wu, J.; Li, X.-L.; Zhao, L.; Guo, M.; Tang, J. Enhancement of Magnetocaloric Effect through Fixation of Carbon Dioxide: Molecular Assembly from $Ln_4$ to $Ln_4$ Cluster Pairs. *Inorg. Chem.* **2017**, *56*, 4104–4111. [CrossRef]
40. Sheldrick, G.M. *SHELXL-2014/7: Program for the Solution of Crystal Structures*; University of Göttingen: Göttingen, Germany, 2014.
41. Bain, G.A.; Berry, J.F. Diamagnetic Corrections and Pascal's Constants. *J. Chem. Educ.* **2008**, *85*, 532–536. [CrossRef]
42. Llunell, M.; Casanova, D.; Cirera, J.; Alemany, P.; Alvarez, S. *SHAPE*, version 2.0; Barcelona, 2010; The program is available upon request from the authors.
43. Chilton, N.F.; Anderson, R.P.; Turner, L.D.; Soncini, A.; Murray, K.S. PHI: A powerful new program for the analysis of anisotropic monomeric and exchange-coupled polynuclear *d*- and *f*-block complexes. *J. Comput. Chem.* **2013**, *34*, 1164–1175. [CrossRef] [PubMed]
44. Thompson, L.K.; Xu, Z.; Goeta, A.E.; Howard, J.A.K.; Clase, H.J.; Miller, D.O. Structural and Magnetic Properties of Dicopper(II) Complexes of Polydentate Diazine Ligands. *Inorg. Chem.* **1998**, *37*, 3217–3229. [CrossRef]
45. Gómez, V.; Corbella, M.; Font-Bardia, M.; Calvet, T. A $\mu_{1,1}$- or $\mu_{1,3}$-carboxylate bridge makes the difference in the magnetic properties of dinuclear MnII compounds. *Dalton Trans.* **2010**, *39*, 11664–11674. [CrossRef] [PubMed]
46. Zhao, L.; Niel, V.; Thompson, L.K.; Xu, Z.; Milway, V.A.; Harvey, R.G.; Miller, D.O.; Wilson, C.; Leech, M.; Howard, J.A.K.; et al. Self-assembled polynuclear clusters derived from some flexible polydentate dihydrazide ligands. *Dalton Trans.* **2004**, 1446–1455. [CrossRef]
47. Thompson, L.K. Polynuclear coordination complexes—From dinuclear to nonanuclear and beyond. *Coord. Chem. Rev.* **2002**, *233–234*, 193–206. [CrossRef]
48. Inoue, M.; Kishita, M.; Kubo, M. Magnetic Moments of Copper(II) Salicylate, Copper(II) Benzoate, and Some Related Compounds. *Inorg. Chem.* **1964**, *3*, 239–242. [CrossRef]
49. Singh, D.P.; Allam, B.K.; Singh, K.N.; Singh, V.P. A binuclear Mn(II) complex as an efficient catalyst for transamidation of carboxamides with amines. *RSC Adv.* **2014**, *4*, 1155–1158. [CrossRef]
50. Nakamoto, K. *Infrared and Raman Spectra of Inorganic and Coordination Compounds*; Wiley: Hoboken, NJ, USA, 2008; ISBN 9780471743392.